

IEM-FT-141/96
 hep-ph/9609392

HIGGS BOSONS IN THE STANDARD MODEL AND THE MINIMAL SUPERSYMMETRIC STANDARD MODEL ^a

M. QUIROS

*Instituto de Estructura de la Materia, Serrano 123,
 28006-Madrid, Spain*

Abstract

In these lectures we present a brief review of the Higgs boson sector in the *Standard Model*, and its Minimal Supersymmetric Extension, with particular emphasis on the main mechanisms for Higgs production and decay at LEP2 and LHC, and theoretical bounds on the Higgs boson masses. In the **Standard Model** the effective potential can develop a non-standard minimum for values of the field much larger than the weak scale. Comparison of the decay rate to the non-standard minimum at finite (and zero) temperature with the corresponding expansion rate of the Universe allows to identify the region, in the (M_H, M_t) -plane which can be accommodated by the theory. In the **Minimal Supersymmetric Standard Model**, approximate analytical expressions for the Higgs mass spectrum and couplings are worked out. An appropriate treatment of squark decoupling allows to consider large values of the stop mixing parameters and thus fix a reliable upper bound on the mass of the lightest CP-even Higgs boson mass. The discovery of the Higgs boson at LEP2 might put an upper bound (below the Planck scale) on the scale of new physics Λ and eventually disentangle between the Standard Model and the Minimal Supersymmetric Standard Model.

IEM-FT-141/95
 September 1995

^aBased on lectures given at the *XXIV INTERNATIONAL MEETING ON FUNDAMENTAL PHYSICS: From Tevatron to LHC*, 22-26 April, 1996, Gandía (Valencia) Spain.

1 Higgs bosons in the Standard Model

In this lecture we will review some elementary and/or well established features of the Higgs sector in the Standard Model (SM)¹. Most of it should be viewed as an introduction for beginners and/or students in the field though we also have presented some recent results on Higgs mass bounds obtained by this author in various collaborations. The methods used to obtain the latter results are sometimes technical. Therefore, we have simplified the analysis and presented only the relevant results.

1.1 Why a Higgs boson?

The Higgs mechanism² is the simplest mechanism to induce spontaneous symmetry breaking of a gauge theory. In particular, in the Standard Model of electroweak interactions it achieves the breaking

$$SU(2)_L \times U(1)_Y \longrightarrow U(1)_{em} \quad (1)$$

in a renormalizable quantum field theory, and gives masses to the gauge bosons W^\pm, Z , the Higgs boson and the fermions.

The SM fermions are given by³

$$\begin{aligned} q_L &= \begin{pmatrix} u_L \\ d_L \end{pmatrix}_{1/6}, \quad (u_R)_{2/3}, \quad (d_R)_{-1/3} \\ \ell_L &= \begin{pmatrix} \nu_L \\ \ell_L \end{pmatrix}_{-1/2}, \quad (\ell_R)_{-1} \end{aligned} \quad (2)$$

where the hypercharge Y is related to the electric charge Q by, $Q = T_3 + Y$, and we are using the notation $f = f_L + f_R$, with

$$\begin{aligned} f_L &= \frac{1}{2}(1 - \gamma_5)f \\ f_R &= \frac{1}{2}(1 + \gamma_5)f. \end{aligned} \quad (3)$$

The Higgs boson is an $SU(2)_L$ doublet, as given by

$$H = \frac{1}{\sqrt{2}} \begin{pmatrix} \chi^+ \\ \Phi + i\chi^0 \end{pmatrix}_{1/2} \quad (4)$$

The physical Higgs ϕ is related to Φ by, $\Phi = \phi + v$, where $v = (\sqrt{2}G_F)^{-1/2} = 246.22$ GeV is the vacuum expectation value (VEV) of the Higgs. The (massless) fields χ^\pm, χ^0 are the Goldstone bosons.

A mass term for gauge bosons V_μ , as $\frac{1}{2}M_V^2 V_\mu V^\mu$ is not gauge invariant, and would spoil the renormalizability properties of the theory. A mass term for fermions, $m_u \bar{q}_L u_R + m_d \bar{q}_L d_R + m_\ell \bar{\ell}_L \ell_R$ does not even exist (it is not $SU(2)_L \times U(1)_Y$ invariant). Both goals can be achieved through the Higgs mechanism².

One can write the part of the SM Lagrangian giving rise to mass terms as

$$\mathcal{L} = (D_\mu H)^\dagger (D_\mu H) - (h_d \bar{q}_L H d_R + h_u \bar{q}_L H^c u_R + h_\ell \bar{\ell}_L H \ell_R + h.c.) - V(H) \quad (5)$$

where $H^c \equiv i\sigma_2 H^*$, the covariant derivative D_μ of the Higgs field is defined by

$$D_\mu H \equiv \left(\partial_\mu + ig \frac{\vec{\sigma}}{2} \vec{W}_\mu + ig' \frac{1}{2} B_\mu \right) H \quad (6)$$

and the Higgs potential by

$$V(H) = -\mu^2 H^\dagger H + \frac{\lambda}{2} (H^\dagger H)^2 \quad (7)$$

Minimization of (7) yields,

$$\langle 0|H|0 \rangle \equiv \frac{v}{\sqrt{2}} \begin{pmatrix} 0 \\ 1 \end{pmatrix}; \quad v = \sqrt{\frac{2\mu^2}{\lambda}} \quad (8)$$

Replacing now $\Phi = \phi + v$ into (5) yields:

$$\begin{aligned} \mathcal{L} = & -\frac{1}{4}g^2 v^2 W_\mu^+ W^{\mu-} - \frac{1}{8}v^2 \begin{pmatrix} Z^\mu & A^\mu \end{pmatrix} \begin{pmatrix} g^2 + g'^2 & 0 \\ 0 & 0 \end{pmatrix} \begin{pmatrix} Z_\mu \\ A_\mu \end{pmatrix} \\ & - \frac{vh_u}{\sqrt{2}} \bar{u}u - \frac{vh_d}{\sqrt{2}} \bar{d}d - \frac{vh_\ell}{\sqrt{2}} \bar{\ell}\ell \end{aligned} \quad (9)$$

where

$$\begin{aligned} W_\mu^\pm &= \frac{1}{\sqrt{2}} (W_{\mu 1} \pm iW_{\mu 2}) \\ Z_\mu &= \cos \theta_W W_{\mu 3} - \sin \theta_W B_\mu \\ A_\mu &= \sin \theta_W W_{\mu 3} + \cos \theta_W B_\mu \end{aligned} \quad (10)$$

and the electroweak angle θ_W is defined by $\tan \theta_W = g'/g$.

In this way the goal of giving masses to the gauge bosons and the fermions has then been achieved as^b

$$M_W^2 = \frac{1}{4}g^2 v^2$$

^bIn the following we will use the notation m_t, m_H for the top-quark and Higgs boson running $\overline{\text{MS}}$ on-shell masses (defined at a scale equal to the corresponding mass), and M_t, M_H for the corresponding pole (physical) masses. They are related by a contribution from self-energies. Thus for the Higgs boson, the running and pole masses are related by⁴ $M_H^2 = m_H^2(M_H) + \text{Re}\Pi_{\phi\phi}(M_H) - \text{Re}\Pi_{\phi\phi}(0)$.

$$\begin{aligned}
M_Z^2 &= \frac{1}{4} (g^2 + g'^2) v^2 \\
m_f &= \frac{1}{\sqrt{2}} h_f v \\
m_H^2 &= \lambda v^2
\end{aligned} \tag{11}$$

1.2 What we know about the Higgs: its couplings

The couplings (g, g', v) are experimentally *traded* by a set of three observables, as e.g. (M_W, M_Z, G_F) , or (α_{em}, M_Z, G_F) , while the Yukawa couplings h_f are *measured* by the fermion masses, m_f . Only the quartic coupling λ in Eq. (5), which should be *measured* by the Higgs mass, is at present **unknown**.

All Higgs interactions (cross-sections, branching ratios,...) are determined once the corresponding Feynman rules are known⁵. In Table 1 we summarize the main vertices involving the physical Higgs boson in the SM along with the rest of particles in the SM.

Vertex	Coupling
$\phi f \bar{f}$	$-i \frac{g}{2M_W} m_f$
$\phi W_\mu^\pm W_\nu^\mp$	$ig M_W g_{\mu\nu}$
$\phi Z_\mu Z_\nu$	$i \frac{g M_Z}{\cos \theta_W} g_{\mu\nu}$
$\phi \phi \phi$	$-i \frac{3g}{2M_W} M_H^2$
$\phi \phi W_\mu^\pm W_\nu^\mp$	$i \frac{1}{2} g^2 g_{\mu\nu}$
$\phi \phi Z_\mu Z_\nu$	$i \frac{1}{2} \frac{g^2}{\cos^2 \theta_W} g_{\mu\nu}$
$\phi \phi \phi \phi$	$-i \frac{3g^2 M_H^2}{4M_W^2}$

Table 1

Higgs production at LEP2

The main mechanisms for production of Higgs particles at e^+e^- colliders, at the LEP2 energies, are⁶:

- **HIGGS-STRAHLUNG:** $e^+e^- \rightarrow Z\phi$, where the Higgs boson is radiated off the virtual Z -boson line exchanged in the s-channel. [Fig. 1, where the solid (fermion) lines are electrons, the wavy line is a Z boson and the dashed line a Higgs ϕ .]

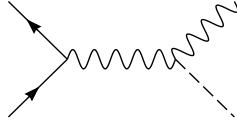


Figure 1: Higgs-strahlung process for Higgs production.

- **WW-FUSION:** $e^+e^- \rightarrow \phi\bar{\nu}_e\nu_e$, where the Higgs boson is formed in the fusion of virtual WW exchanged in the t-channel. The virtual W 's are radiated off the electron and positron of the beam. [Fig. 2, where the incoming lower (upper) fermion line is an electron (positron) and the corresponding outgoing fermion a ν_e ($\bar{\nu}_e$). Wavy lines are W and the dashed line a Higgs.]

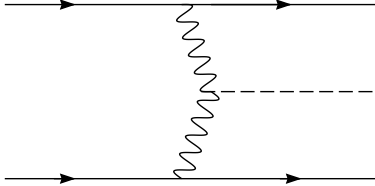


Figure 2: Vector-Vector fusion process for Higgs production.

A detailed analysis of these processes for LEP2 can be found in Ref. ⁶. There it is found that the Higgs-strahlung process dominates the cross-section for low values of the Higgs mass ($M_H < 105$ GeV), while the WW-fusion process dominates it for large values of the Higgs mass ($M_H > 105$ GeV).

Higgs production at LHC

The main mechanisms for production of Higgs bosons at pp colliders, at the LHC energies, are ⁷:

- **GLUON-GLUON FUSION:** $gg \rightarrow \phi$, where two gluons in the sea of the protons collide through a loop of top-quarks, which subsequently emits a

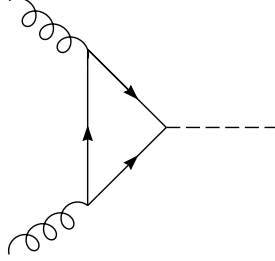


Figure 3: Gluon-gluon fusion process for Higgs production.

Higgs boson. [Fig. 3 where the curly lines are gluons, the internal fermion line a top and the dashed line a Higgs.]

- WW (ZZ)-FUSION: $W^\pm W^\mp(ZZ) \rightarrow \phi$, where the Higgs boson is formed in the fusion of $WW(ZZ)$, the virtual $W(Z)$'s being exchanged in the t-channel and radiated off a quark in the proton beam. [Fig. 2, where wavy lines are $W(Z)$, the incoming fermions quarks q and the outgoing fermions quarks $q(q')$. The dashed line is the Higgs.]
- HIGGS STRAHLUNG: $q\bar{q}^{(\prime)} \rightarrow Z(W)\phi$, where the Higgs boson is radiated off the virtual $Z(W)$ -boson line exchanged in the s-channel. [Fig. 1, where wavy lines are $Z(W)$, the incoming fermion a quark q and the outgoing fermion a quark $q(q')$.]
- ASSOCIATED PRODUCTION WITH $t\bar{t}$: $gg \rightarrow \phi t\bar{t}$, where the gluons from the proton sea exchange a top quark in the t-channel, which emits a Higgs boson. [Fig. 4, where curly lines are gluons and the fermion line corresponds to a quark t . The dashed line is the Higgs boson.]

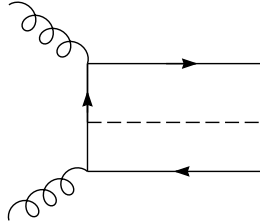


Figure 4: Associated production of Higgs with $f\bar{f}$.

A complete analysis of the different production channels can be found, e.g. in Ref. ⁸. It is found that for a top mass in the experimental range ⁹ the gluon-gluon fusion mechanism is dominating the production cross-section for any value of the Higgs mass. The subdominant process, WW(ZZ)-fusion is comparable in magnitude to the gluon-gluon process only for very large values of the Higgs mass $M_H \sim 1$ TeV. For low values of the Higgs mass, $M_H \sim 100$ GeV, the gluon-gluon fusion process is still dominant over all other channels by around one order of magnitude, while all the others are similar in magnitude for these values of the Higgs mass.

Higgs decays

For values of the Higgs mass relevant at LEP2 energies, the main decay modes of the Higgs boson are:

- $\phi \rightarrow b\bar{b}, c\bar{c}, \tau^-\tau^+$, which is dominated by the $b\bar{b}$ channel.
- $\phi \rightarrow gg$, where the gluons are produced by a top-quark loop emitted by the Higgs. [The inverse diagram of Fig. 3.]
- $\phi \rightarrow WW^* \rightarrow Wf\bar{f}'$, which is relevant for values of the Higgs mass, $M_H > M_W$.

A complete analysis of different Higgs decay channels reveals ⁶ that, for LEP2 range of Higgs masses, $M_H < 110$ GeV, the $b\bar{b}$ channel dominates the Higgs branching ratio by \sim one order of magnitude.

For $M_H > 110$ GeV, the main decay modes relevant for LHC energies and pp colliders are ⁸:

- $\phi \rightarrow \gamma\gamma$, where the photons are produced by a top-quark loop emitted by the Higgs. [The inverse diagram as that of Fig. 3, where gluons are replaced by photons.]
- $\phi \rightarrow W^\pm W^\mp$, which requires $M_H > 2M_W$.
- $\phi \rightarrow ZZ$, which requires $M_H > 2M_Z$.
- $\phi \rightarrow t\bar{t}$, which requires $M_H > 2M_t$.

For a heavy Higgs ($M_H > 150$ GeV) the WW(ZZ) decay channels completely dominate the Higgs branching ratio, while the radiative decay $\gamma\gamma$ dominates for low values of the Higgs mass and is expected to close the LHC window for a light Higgs. The reader is referred to Ref. ⁸ for more details.

1.3 What we do not know about the Higgs: its mass

Being the Higgs boson the missing ingredient of the SM, the quartic coupling λ , and so its mass, are unknown. However we can have information on M_h from experimental and theoretical input.

From experimental inputs we have direct and indirect information on the Higgs mass. Since direct experimental searches at LEP have been negative up to now, they translate into a lower bound on the Higgs mass¹⁰,

$$M_h > 67 \text{ GeV}, \quad (12)$$

Experimental searches also yield indirect information, which is the influence the Higgs mass has in radiative corrections and in precision measurements at LEP¹⁰. However, unlike the top quark mass, on which the radiative corrections are quadratically dependent, and so very sensitive, the dependence of one-loop radiative corrections on the Higgs mass is only logarithmic (the so-called Veltman's screening theorem), which means that radiative corrections in the SM have very little sensitivity to the Higgs mass, providing only very loose bounds from precision measurements.

However, from the theoretical input the situation is rather different. In fact the theory has a lot of information on M_h , which can be used to put bounds on the Higgs mass. If these bounds were evaded when the Higgs mass will be eventually measured, this measurement might lead to the requirement of new physics, just because the SM cannot accomodate such a value of the Higgs (and the top-quark) mass.

For particular values of the Higgs boson and top quark masses, M_H and M_t , the effective potential of the Standard Model (SM) develops a deep non-standard minimum for values of the field $\phi \gg G_F^{-1/2}$ ¹¹. In that case the standard electroweak (EW) minimum becomes metastable and might decay into the non-standard one. This means that the SM might have troubles in certain regions of the plane (M_H, M_t) , a fact which can be intrinsically interesting as evidence for new physics. Of course, the mere existence of the non-standard minimum, and also the decay rate of the standard one into it, depends on the scale Λ up to which we believe the SM results. In fact, one can identify Λ with the scale of new physics.

Stability bounds

The preliminary question one should ask is: When the standard EW minimum becomes metastable, due to the appearance of a deep non-standard minimum? This question was addressed in past years¹¹ taking into account leading-log

(LL) and part of next-to-leading-log (NTLL) corrections. More recently, calculations have incorporated all NTLL corrections^{12,13} resummed to all-loop by the renormalization group equations (RGE), and considered pole masses for the top-quark and the Higgs-boson. From the requirement of a stable (not metastable) standard EW minimum we obtain a lower bound on the Higgs mass, as a function of the top mass, labelled by the values of the SM cutoff (stability bounds). Our result¹³ is lower than previous estimates by $\mathcal{O}(10)$ GeV. The problem to attack is easily stated as follows:

The effective potential in the SM can be written as (7)

$$V = -\frac{1}{2}m^2\phi^2 + \frac{1}{8}\lambda\phi^4 + \dots \quad (13)$$

where the ellipsis refers to radiative corrections and all parameters and fields in (13) are running with the renormalization group scale $\mu(t) = M_Z \exp(t)$. The condition for having an extremal is $V'(\phi(t)) = 0$, which has as solution

$$\phi^2 = \frac{2m^2}{\lambda - \frac{12}{32\pi^2}h_t^4 \left(\log \frac{h_t^2\phi^2}{2\mu^2} - 1 \right)} \quad (14)$$

where h_t refers to the top Yukawa coupling, and only the leading radiative corrections have been kept for simplicity. The curvature of the potential (13) at the extreme is given by

$$V''(\phi) = 2m^2 + \frac{1}{2}\beta_\lambda\phi^2 \quad (15)$$

The condition $V' = 0$ is obviously satisfied at the EW minimum where $\langle\phi\rangle = v \sim 246$ GeV, $\lambda \sim (m_H/v)^2 > 1/16$, $m^2 \sim m_H^2/2$ and $V''(\langle\phi\rangle) > 0$ (a minimum). However, the condition $V' = 0$ can also be satisfied for values of the field $\phi \gg v$ and, since $m = \mathcal{O}(100)$ GeV, for those values

$$\lambda \sim \left(\frac{m}{\phi} \right)^2 \ll 1.$$

Therefore, for the non-standard extremals we have

$$\begin{aligned} \beta_\lambda < 0 &\implies V'' < 0 \text{ maximum} \\ \beta_\lambda > 0 &\implies V'' > 0 \text{ minimum.} \end{aligned} \quad (16)$$

The one-loop effective potential of the SM improved by two-loop RGE has been shown to be highly scale independent⁴ and, therefore, very reliable for

the present study. In Fig. 5 we show (thick solid line) the shape of the effective potential for $M_t = 175$ GeV and $M_H = 121.7$ GeV. We see the appearance of the non-standard maximum, ϕ_M , while the global non-standard minimum has been cutoff at M_{Pl} . We can see from Fig. 5 the steep descent from the non-standard maximum. Hence, even if the non-standard minimum is beyond the SM cutoff, the standard minimum becomes metastable and might be destabilized. So for fixed values of M_H and M_t the condition for the standard minimum not to become metastable is

$$\phi_M \gtrsim \Lambda \quad (17)$$

Condition (17) makes the stability condition Λ -dependent. In fact we have plotted in Fig. 6 the stability condition on M_H versus M_t for $\Lambda = 10^{19}$ GeV and 10 TeV. The stability region corresponds to the region above the dashed curves.

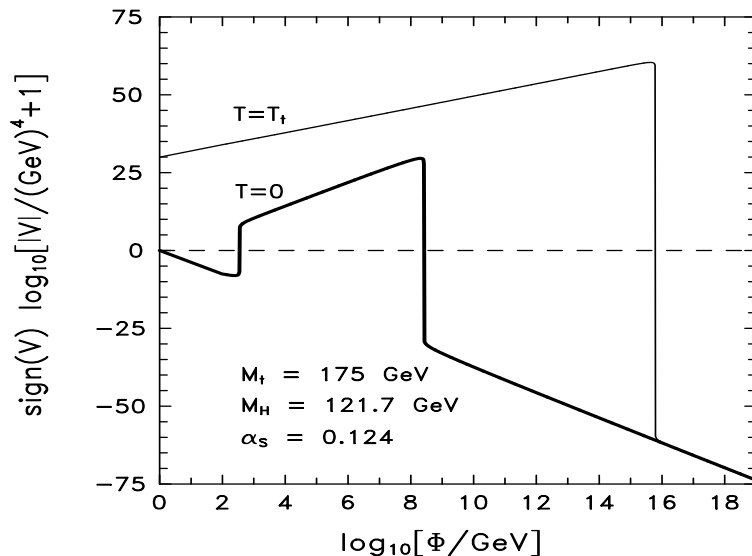


Figure 5: Plot of the effective potential for $M_t = 175$ GeV, $M_H = 121.7$ GeV at $T = 0$ (thick solid line) and $T = T_t = 2.5 \times 10^{15}$ GeV (thin solid line).

Metastability bounds

In the last subsection we have seen that in the region of Fig. 6 below the dashed line the standard EW minimum is metastable. However we should not

draw physical consequences from this fact since we still do not know at which minimum does the Higgs field sit. Thus, the real physical constraint we have to impose is avoiding the Higgs field sitting at its non-standard minimum. In fact the Higgs field can be sitting at its zero temperature non-standard minimum because:

1. The Higgs field was driven from the origin to the non-standard minimum at finite temperature by thermal fluctuations in a non-standard EW phase transition at high temperature. This minimum evolves naturally to the non-standard minimum at zero temperature. In this case the standard EW phase transition, at $T \sim 10^2$ GeV, will not take place.
2. The Higgs field was driven from the origin to the standard minimum at $T \sim 10^2$ GeV, but decays, at zero temperature, to the non-standard minimum by a quantum fluctuation.

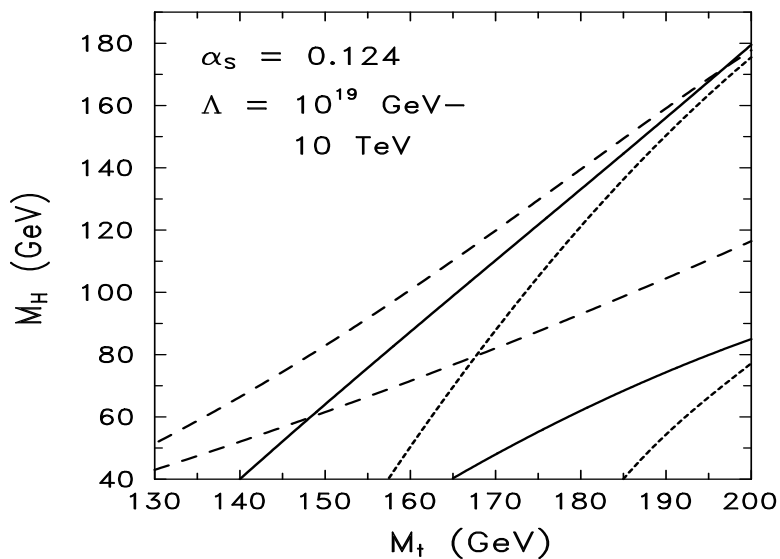


Figure 6: Lower bounds on M_H as a function of M_t , for $\Lambda = 10^{19}$ GeV (upper set) and $\Lambda = 10$ TeV (lower set). The dashed curves correspond to the stability bounds and the solid (dotted) ones to the metastability bounds at finite (zero) temperature.

In Fig. 5 we have depicted the effective potential at $T = 2.5 \times 10^{15}$ GeV (thin solid line) which is the corresponding transition temperature. Our finite temperature potential¹⁴ incorporates plasma effects¹⁵ by one-loop resummation

of Debye masses¹⁶. The tunnelling probability per unit time per unit volume was computed long ago for thermal¹⁷ and quantum¹⁸ fluctuations. At finite temperature it is given by $\Gamma/\nu \sim T^4 \exp(-S_3/T)$, where S_3 is the euclidean action evaluated at the bounce solution $\phi_B(0)$. The semiclassical picture is that unstable bubbles are nucleated behind the barrier at $\phi_B(0)$ with a probability given by Γ/ν . Whether or not they fill the Universe depends on the relation between the probability rate and the expansion rate of the Universe. By normalizing the former with respect to the latter we obtain a normalized probability P , and the condition for decay corresponds to $P \sim 1$. Of course our results are trustable, and the decay actually happens, only if $\phi_B(0) < \Lambda$, so that the similar condition to (17) is

$$\Lambda < \phi_B(0) \quad (18)$$

The condition of no-decay (metastability condition) has been plotted in Fig. 6 (solid lines) for $\Lambda = 10^{19}$ GeV and 10 TeV. The region between the dashed and the solid line corresponds to a situation where the non-standard minimum exists but there is no decay to it at finite temperature. In the region below the solid lines the Higgs field is sitting already at the non-standard minimum at $T \sim 10^2$ GeV, and the standard EW phase transition does not happen.

We also have evaluated the tunnelling probability at zero temperature from the standard EW minimum to the non-standard one. The result of the calculation should translate, as in the previous case, in lower bounds on the Higgs mass for different values of Λ . The corresponding bounds are shown in Fig. 6 in dotted lines. Since the dotted lines lie always below the solid ones, the possibility of quantum tunnelling at zero temperature does not impose any extra constraint.

As a consequence of all improvements in the calculation, our bounds are lower than previous estimates¹⁹. To fix ideas, for $M_t = 175$ GeV, the bound reduces by ~ 10 GeV for $\Lambda = 10^4$ GeV, and ~ 30 GeV for $\Lambda = 10^{19}$ GeV.

Perturbativity bounds

Up to here we have described lower bounds on the Higgs mass based on stability arguments. Another kind of bounds, which have been used in the literature, are upper bounds based on the requirement of perturbativity of the SM up to the high scale (the scale of new physics) Λ .

Since the quartic coupling grows with the scale^c, it will blow up to infinity at a given scale: the scale where λ has a Landau pole. The position of the

^cIn fact the value of the renormalization scale where the quartic coupling starts growing depends on the value of the top-quark mass.

Landau pole Λ is, by definition, the maximum scale up to which the SM is perturbatively valid. In this way assuming the SM remains valid up to a given scale Λ amounts to requiring an upper bound on the Higgs mass from the perturbativity condition⁶

$$\frac{\lambda(\Lambda)}{4\pi} \leq 1 \quad (19)$$

This upper bound depends on the scale Λ and very mildly on the top-quark mass M_t through its influence on the renormalization group equations of λ . We have plotted in Fig. 7 this upper bound for different values of the high scale Λ , along with the corresponding stability bounds.

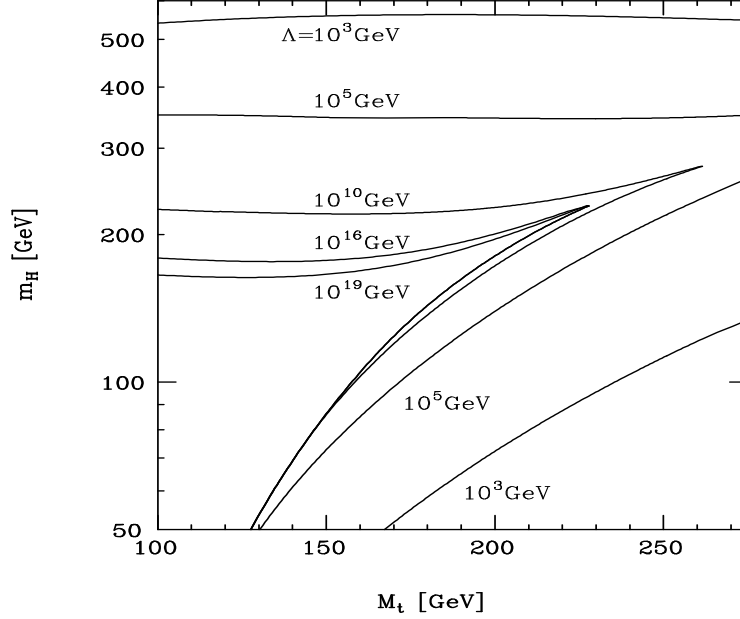


Figure 7: Perturbativity and stability bounds on the SM Higgs boson. Λ denotes the energy scale where the particles become strongly interacting.

1.4 A light Higgs can measure the scale of New Physics

From the bounds on $M_H(\Lambda)$ previously obtained (see Fig. 8) one can easily deduce that a measurement of M_H might provide an **upper bound** (below the Planck scale) on the scale of new physics provided that

$$M_t > \frac{M_H}{2.25 \text{ GeV}} + 123 \text{ GeV} \quad (20)$$

Thus, the present experimental bound from LEP, $M_H > 67 \text{ GeV}$, would imply, from (20), $M_t > 153 \text{ GeV}$, which is fulfilled by experimental detection of the top⁹. Even non-observation of the Higgs at LEP2 (i.e. $M_H \gtrsim 95 \text{ GeV}$), would leave an open window ($M_t \gtrsim 165 \text{ GeV}$) to the possibility that a future Higgs detection at LHC could lead to an upper bound on Λ . Moreover, Higgs detection at LEP2 would put an upper bound on the scale of new physics.

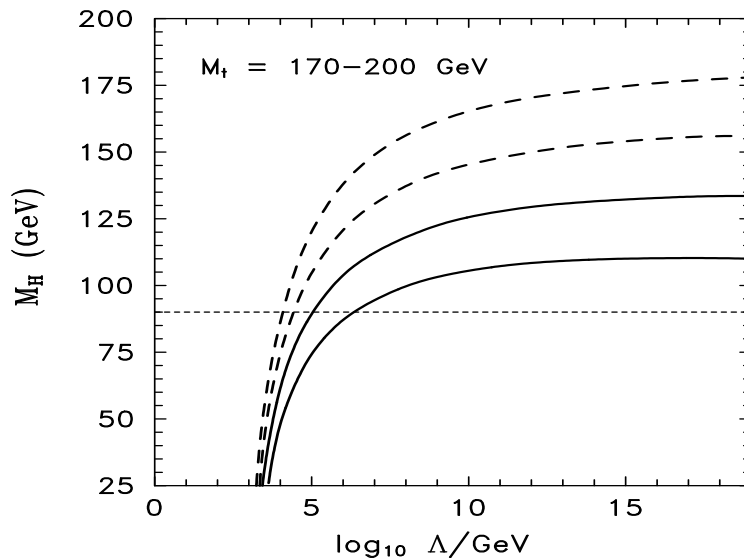


Figure 8: SM lower bounds on M_H from metastability requirements as a function of Λ for different values of M_t .

Taking, for instance, $M_H \lesssim 95 \text{ GeV}$ and $170 \text{ GeV} < M_t < 180 \text{ GeV}$, then $\Lambda \lesssim 10^7 \text{ GeV}$, while for $180 \text{ GeV} < M_t < 190 \text{ GeV}$, $\Lambda \lesssim 10^4 \text{ GeV}$, as can be deduced from Fig. 8. Finally, using as upper bound for the top-quark mass $M_t < 180 \text{ GeV}$ [Ref.⁹] we obtain from (20) that only if the condition

$$M_h > 128 \text{ GeV} \quad (21)$$

is fulfilled, the SM can be a consistent theory up to the Planck scale, where gravitational effects can no longer be neglected.

2 Higgs bosons in the Minimal Supersymmetric Standard Model

The Minimal Supersymmetric Standard Model (MSSM) ²⁰ is the best motivated extension of the SM where some of their theoretical problems (e.g. the hierarchy problem inherent with the fact that the SM cannot be considered as a fundamental theory for energies beyond the Planck scale) find at least a technical solution ²¹. In this lecture we will concentrate on the Higgs sector of the MSSM that is being the object of experimental searches at present accelerators (LEP), and will equally be one of the main goals at future colliders (LHC).

2.1 The Higgs sector in the Minimal Supersymmetric Standard Model

The Higgs sector of the MSSM ²² requires two Higgs doublets, with opposite hypercharges, as

$$H_1 = \begin{pmatrix} H_1^0 \\ H_1^- \end{pmatrix}_{-1/2}, \quad H_2 = \begin{pmatrix} H_2^+ \\ H_2^0 \end{pmatrix}_{1/2} \quad (22)$$

The reason for this duplicity is twofold. On the one hand it is necessary to cancel the triangular anomalies generated by the higgsinos. On the other hand it is required by the structure of the supersymmetric theory to give masses to all fermions.

The most general gauge invariant scalar potential is given, for a general two-Higgs doublet model, by:

$$\begin{aligned} V = & m_1^2 |H_1|^2 + m_2^2 |H_2|^2 + (m_3^2 H_1 H_2 + h.c.) + \frac{1}{2} \lambda_1 (H_1^\dagger H_1)^2 \\ & + \frac{1}{2} \lambda_2 (H_2^\dagger H_2)^2 + \lambda_3 (H_1^\dagger H_1)(H_2^\dagger H_2) + \lambda_4 (H_1 H_2)(H_1^\dagger H_2^\dagger) \\ & + \left\{ \frac{1}{2} \lambda_5 (H_1 H_2)^2 + \left[\lambda_6 (H_1^\dagger H_1) + \lambda_7 (H_1^\dagger H_2^\dagger) \right] (H_1 H_2) + h.c. \right\} \end{aligned} \quad (23)$$

However, supersymmetry provides the following tree-level relations between the previous couplings. The non-vanishing ones are:

$$\lambda_1 = \lambda_2 = \frac{1}{4}(g^2 + g'^2), \quad \lambda_3 = \frac{1}{4}(g^2 - g'^2), \quad \lambda_4 = -\frac{1}{4}g^2 \quad (24)$$

Replacing (24) into (23) one obtains the tree-level potential of the MSSM, as:

$$V_{\text{MSSM}} = m_1^2 H_1^\dagger H_1 + m_2^2 H_2^\dagger H_2 + m_3^2 (H_1 H_2 + h.c.) + \frac{1}{8} g^2 \left(H_2^\dagger \vec{\sigma} H_2 + H_1^\dagger \vec{\sigma} H_1 \right)^2 + \frac{1}{8} g'^2 \left(H_2^\dagger H_2 - H_1^\dagger H_1 \right)^2 \quad (25)$$

This potential, along with the gauge and Yukawa couplings in the superpotential,

$$W = h_u Q \cdot H_2 U^c + h_d Q \cdot H_1 D^c + h_\ell L \cdot H_1 E^c + \mu H_1 \cdot H_2 \quad (26)$$

determine all couplings and masses (at the tree-level) of the Higgs sector in the MSSM.

After gauge symmetry breaking,

$$\begin{aligned} v_1 &= \langle \text{Re } H_1^0 \rangle \\ v_2 &= \langle \text{Re } H_2^0 \rangle \end{aligned} \quad (27)$$

the Higgs spectrum contains one neutral CP-odd Higgs A (with mass m_A , that will be taken as a free parameter)

$$A = \cos \beta \text{Im} H_2^0 + \sin \beta \text{Im} H_1^0 \quad (28)$$

and one neutral Goldstone χ^0

$$\chi^0 = -\sin \beta \text{Im} H_2^0 + \cos \beta \text{Im} H_1^0 \quad (29)$$

with $\tan \beta = v_2/v_1$. It also contains one complex charged Higgs H^\pm ,

$$H^+ = \cos \beta H_2^+ + \sin \beta (H_1^-)^* \quad (30)$$

with a (tree-level) mass

$$m_{H^\pm}^2 = M_W^2 + m_A^2 \quad (31)$$

and one charged Goldstone χ^\pm ,

$$\chi^+ = -\sin \beta H_2^+ + \cos \beta (H_1^-)^*. \quad (32)$$

Finally the Higgs spectrum contains two CP-even neutral Higgs bosons H, \mathcal{H} (the light and the heavy mass eigenstates) which are linear combinations of $\text{Re } H_1^0$ and $\text{Re } H_2^0$, with a mixing angle α given by

$$\cos 2\alpha = -\cos 2\beta \frac{m_A^2 - M_Z^2}{m_{\mathcal{H}}^2 - m_H^2} \quad (33)$$

and masses

$$m_{H, \mathcal{H}}^2 = \frac{1}{2} \left[m_A^2 + M_Z^2 \mp \sqrt{(m_A^2 + M_Z^2)^2 - 4m_A^2 M_Z^2 \cos^2 2\beta} \right] \quad (34)$$

The Higgs couplings

All couplings in the Higgs sector are functions of the gauge (G_F, g, g') and Yukawa couplings, as in the SM, and of the previously defined mixing angles β, α . Some relevant couplings are contained in Table 2 where all particle momenta, in squared brackets, are incoming.

Vertex	Couplings
$(H, \mathcal{H})WW$	$(\phi WW)_{\text{SM}}[\sin(\beta - \alpha), \cos(\beta - \alpha)]$
$(H, \mathcal{H})ZZ$	$(\phi ZZ)_{\text{SM}}[\sin(\beta - \alpha), \cos(\beta - \alpha)]$
$(H, \mathcal{H}, A)[p]W^\pm H^\mp[k]$	$\mp i\frac{g}{2}(p+k)^\mu[\cos(\beta - \alpha), -\sin(\beta - \alpha), \pm i]$
$(H, \mathcal{H}, A)u\bar{u}$	$(\phi u\bar{u})_{\text{SM}}[\frac{\cos \alpha}{\sin \beta}, \frac{\sin \alpha}{\sin \beta}, -i\gamma_5 \cot \beta]$
$(H, \mathcal{H}, A)d\bar{d}$	$(\phi d\bar{d})_{\text{SM}}[-\frac{\sin \alpha}{\cos \beta}, \frac{\cos \alpha}{\cos \beta}, -i\gamma_5 \tan \beta]$
$H^-u\bar{d}$	$\frac{ig}{2\sqrt{2}M_W}[(m_d \tan \beta + m_u \cot \beta) - (m_d \tan \beta - m_u \cot \beta)\gamma_5]$
$H^+\bar{u}d$	$\frac{ig}{2\sqrt{2}M_W}[(m_d \tan \beta + m_u \cot \beta) + (m_d \tan \beta - m_u \cot \beta)\gamma_5]$
$(\gamma, Z)H^+[p]H^-[k]$	$-i(p+k)^\mu \left[e, g\frac{\cos 2\theta_W}{2\cos \theta_W} \right]$
$h[p]A[k]Z$	$-\frac{e}{2\cos \theta_W \sin \theta_W}(p+k)^\mu \cos(\beta - \alpha)$

Table 2

Higgs production at LEP2

The main mechanisms for production of neutral Higgs particles at e^+e^- colliders, at the LEP2 energies, are⁶:

- **HIGGS-STRAHLUNG:** $e^+e^- \rightarrow ZH$, where the Higgs boson is radiated off the virtual Z -boson line. This process is identical to the SM Higgs-strahlung. [See Fig. 1.]
- **ASSOCIATED PAIR PRODUCTION:** $e^+e^- \rightarrow HA$, $e^+e^- \rightarrow H^\pm H^\mp$. The production of HA is mediated by a Z -boson in the s-channel (it uses the coupling hAZ in Table 2). The production of $H^\pm H^\mp$ can be mediated by either γ and Z , using the $(\gamma, Z)H^\pm H^\mp$ vertex in Table 2.

A detailed analysis of these processes for LEP2 can be found in Ref. ⁶.

Higgs production at LHC

The main mechanisms for production of neutral Higgs bosons at pp colliders, at the LHC energies, are ⁷:

- **GLUON-GLUON FUSION:** $gg \rightarrow (H, \mathcal{H}, A)$, where two gluons in the sea of the protons collide through a loop of top-quarks, bottom-quarks, stops and sbottoms which subsequently emit a Higgs boson. The contribution of a (s)bottom loop is only relevant for large values of $\tan\beta$. [Figs. 3 and 9, where curly lines are gluons, internal fermion lines quarks t and b , internal boson (dashed) lines squarks \tilde{t} and \tilde{b} and the dashed line is a Higgs boson H , \mathcal{H} or A .]

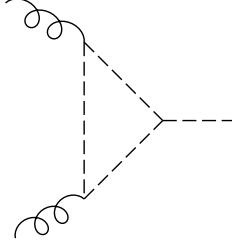


Figure 9: Gluon-gluon fusion process for Higgs production with a squark loop.

- **WW (ZZ)-FUSION:** $W^\pm W^\mp \rightarrow (H, \mathcal{H}, A)$, $ZZ \rightarrow (H, \mathcal{H}, A)$, where the Higgs boson is formed in the fusion of $WW(ZZ)$, the virtual $W(Z)$'s being radiated off a quark in the proton beam. [See Fig. 2 where the external dashed line corresponds to a Higgs boson H , \mathcal{H} or A .]
- **HIGGS STRAHLUNG:** $q\bar{q} \rightarrow Z(H, \mathcal{H}, A)$, $q\bar{q}' \rightarrow W(H, \mathcal{H}, A)$ where the corresponding Higgs boson is radiated off the virtual $Z(W)$ -boson line. [See Fig. 1, where the dashed line is a Higgs boson, H , \mathcal{H} or A .]

- ASSOCIATED PRODUCTION WITH $t\bar{t}, b\bar{b}$: $gg \rightarrow t\bar{t}(H, \mathcal{H}, A)$, $gg \rightarrow b\bar{b}(H, \mathcal{H}, A)$ where the gluons from the proton sea exchange a top (bottom)-quark in the t-channel, the exchanged top (bottom) quark emitting a Higgs boson. [See Fig. 4 where the curly lines are gluons, the fermion line a t or b quark and the dashed line a Higgs boson H, \mathcal{H} or A .]

The production of a charged Higgs boson is through the process $gg \rightarrow t\bar{t}$, where the gluons exchange a top-quark in the t-channel, and subsequent decay $t \rightarrow bH^+$. This process is available only when $M_t > m_{H^+} + M_b$. Otherwise the detection of the charged Higgs is much more difficult. [Fig. 10 where curly lines are gluons, the fermion exchanged between the gluons a t quark, the external fermions b quarks and the external bosons (dashed) are H^\pm .] A complete analysis of the different production channels can be found, e.g. in Ref. ²³.

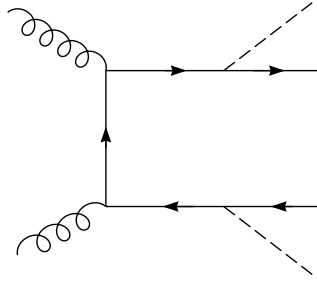


Figure 10: Charged higgs production process.

Higgs decays

Assuming R-parity conservation, two-body decays should be into SM particles, or two supersymmetric partners if the supersymmetric spectrum is kinematically accessible. Assuming the supersymmetric spectrum to be heavy enough (a useful working hypothesis), the decays are always into SM particles. The main decay modes of the Higgs boson are then:

- $(H, \mathcal{H}, A) \rightarrow b\bar{b}, c\bar{c}, \tau^-\tau^+, t\bar{t}, gg, \gamma\gamma, W^*W^*, Z^*Z^*, Z\gamma$, which is very similar to the corresponding SM modes.
- $H \rightarrow AA$.
- $\mathcal{H} \rightarrow hh, AA, ZA$.

- $A \rightarrow ZH$:
- $H^+ \rightarrow c\bar{s}, \tau^+\nu_\tau, t\bar{b}, W^+H$.

A complete analysis of the decay modes in the MSSM can be found in Ref. ⁶, for LEP2, and ²³ for LHC.

2.2 Radiative corrections

All previous Higgs production and decay processes depend on the Higgs masses $m_H, m_{\mathcal{H}}, m_A, m_{H^\pm}$, and couplings $g, g', G_F, \tan\beta, \cos\alpha, h_f, \lambda_1, \dots, \lambda_7$. We have already given their tree-level values. In particular, the mass spectrum satisfies at tree-level the following relations:

$$\begin{aligned} m_H &< M_Z |\cos 2\beta| \\ m_H &< m_A \\ m_{H^\pm} &> M_W \end{aligned} \tag{35}$$

which could have a number of very important phenomenological implications, as it is rather obvious. However, it was discovered that radiative corrections are important and can spoil the above tree level relations with a great phenomenological relevance. A detailed knowledge of radiatively corrected couplings and masses is necessary for experimental searches in the MSSM.

The **effective potential** methods to compute the (radiatively corrected) Higgs mass spectrum in the MSSM are useful since they allow to **resum** (using Renormalization Group (RG) techniques) LL, NTLL,..., corrections to **all orders** in perturbation theory. These methods ^{24,25}, as well as the diagrammatic methods ²⁶ to compute the Higgs mass spectrum in the MSSM, were first developed in the early nineties.

Effective potential methods are based on the **run-and-match** procedure by which all dimensionful and dimensionless couplings are running with the RG scale, for scales greater than the masses involved in the theory. When the RG scale equals a particular mass threshold, heavy fields decouple, eventually leaving threshold effects in order to match the effective theory below and above the mass threshold. For instance, assuming a common soft supersymmetry breaking mass for left-handed and right-handed stops and sbottoms, $M_S \sim m_Q \sim m_U \sim m_D$, and assuming for the top-quark mass, m_t , and for the CP-odd Higgs mass, m_A , the range $m_t \leq m_A \leq M_S$, we have: for scales $Q \geq M_S$, the MSSM, for $m_A \leq Q \leq M_S$ the two-Higgs doublet model (2HDM), and for $m_t \leq Q \leq m_A$ the SM. Of course there are thresholds effects at $Q = M_S$ to match the MSSM with the 2HDM, and at $Q = m_A$ to match the 2HDM with the SM.

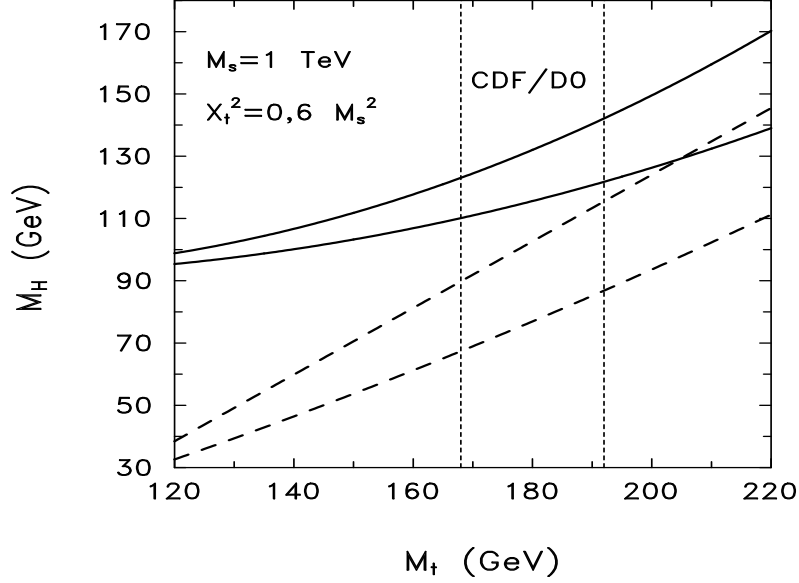


Figure 11: Plot of M_H as a function of M_t for $\tan \beta \gg 1$ (solid lines), $\tan \beta = 1$ (dashed lines), and $X_t^2 = 6M_S^2$ (upper set), $X_t = 0$ (lower set). The experimental band from the CDF/D0 detection is also indicated.

As we have said, the neutral Higgs sector of the MSSM contains, on top of the CP-odd Higgs A , two CP-even Higgs mass eigenstates, \mathcal{H} (the heaviest one) and H (the lightest one). It turns out that the larger m_A the heavier the lightest Higgs H . Therefore the case $m_A \sim M_S$ is, not only a great simplification since the effective theory below M_S is the SM, but also of great interest, since it provides the upper bound on the mass of the lightest Higgs (which is interesting for phenomenological purposes, e.g. at LEP2). In this case the threshold correction at M_S for the SM quartic coupling λ is:

$$\Delta_{\text{th}}\lambda = \frac{3}{16\pi^2}h_t^4 \frac{X_t^2}{M_S^2} \left(2 - \frac{1}{6} \frac{X_t^2}{M_S^2} \right) \quad (36)$$

where h_t is the SM top Yukawa coupling and $X_t = (A_t - \mu/\tan \beta)$ is the mixing in the stop mass matrix, the parameters A_t and μ being the trilinear soft-breaking coupling in the stop sector and the supersymmetric Higgs mixing mass, respectively. The maximum of (36) corresponds to $X_t^2 = 6M_S^2$ which provides the maximum value of the lightest Higgs mass: this case will be referred to as the case of maximal mixing.

We have plotted in Fig. 11 the lightest Higgs pole mass M_H , where all NTLL corrections are resummed to all-loop by the RG, as a function of M_t ⁴. From Fig. 11 we can see that the present experimental band from CDF/D0 for the top-quark mass requires $M_H \lesssim 140$ GeV, while if we fix $M_t = 170$ GeV, the upper bound $M_H \lesssim 125$ GeV follows. It goes without saying that these figures are extremely relevant for MSSM Higgs searches at LEP2.

An analytical approximation

We have seen⁴ that, since radiative corrections are minimized for scales $Q \sim m_t$, when the LL RG improved Higgs mass expressions are evaluated at the top-quark mass scale, they reproduce the NTLL value with a high level of accuracy, for any value of $\tan \beta$ and the stop mixing parameters²⁷

$$m_{H,LL}(Q^2 \sim m_t^2) \sim m_{H,NTLL}. \quad (37)$$

Based on the above observation, we can work out a very accurate analytical approximation to $m_{H,NTLL}$ by just keeping two-loop LL corrections at $Q^2 = m_t^2$, i.e. corrections of order t^2 , where $t = \log(M_S^2/m_t^2)$.

Again the case $m_A \sim M_S$ is the simplest, and very illustrative, one. We have found^{27,28} that, in the absence of mixing (the case $X_t = 0$) two-loop corrections resum in the one-loop result shifting the energy scale from M_S (the tree-level scale) to $\sqrt{M_S m_t}$. More explicitly,

$$m_H^2 = M_Z^2 \cos^2 2\beta \left(1 - \frac{3}{8\pi^2} h_t^2 t \right) + \frac{3}{2\pi^2 v^2} m_t^4 (\sqrt{M_S m_t}) t \quad (38)$$

where $v = 246.22$ GeV.

In the presence of mixing ($X_t \neq 0$), the run-and-match procedure yields an extra piece in the SM effective potential $\Delta V_{\text{th}}[\phi(M_S)]$ whose second derivative gives an extra contribution to the Higgs mass, as

$$\Delta_{\text{th}} m_H^2 = \frac{\partial^2}{\partial \phi^2(t)} \Delta V_{\text{th}}[\phi(M_S)] = \frac{1}{\xi^2(t)} \frac{\partial^2}{\partial \phi^2(t)} \Delta V_{\text{th}}[\phi(M_S)] \quad (39)$$

which, in our case, reduces to

$$\Delta_{\text{th}} m_H^2 = \frac{3}{4\pi^2} \frac{m_t^4(M_S)}{v^2(m_t)} \frac{X_t^2}{M_S^2} \left(2 - \frac{1}{6} \frac{X_t^2}{M_S^2} \right) \quad (40)$$

We have compared our analytical approximation²⁷ with the numerical NTLL result⁴ and found a difference $\lesssim 2$ GeV for all values of supersymmetric parameters.

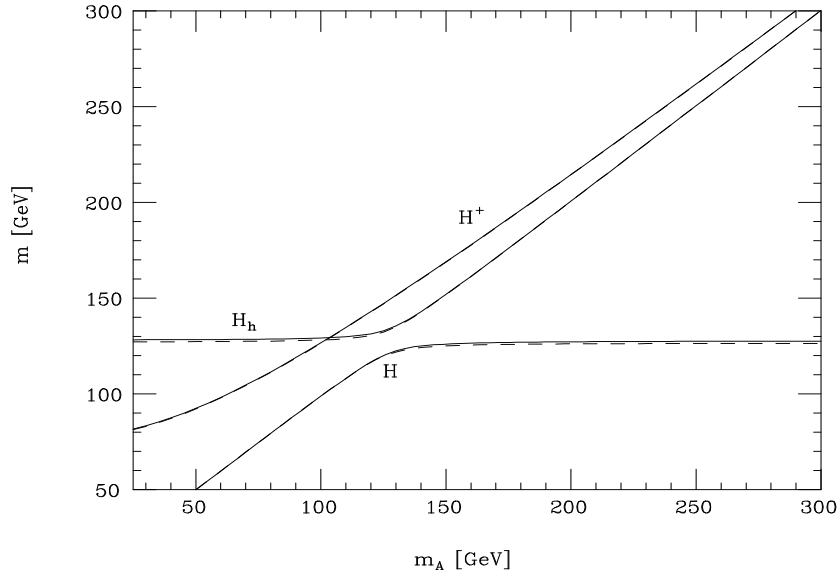


Figure 12: The neutral ($H, \mathcal{H} \equiv H_h$ in the figure) and charged (H^+) Higgs mass spectrum as a function of the CP-odd Higgs mass m_A for a physical top-quark mass $M_t = 175$ GeV and $M_S = 1$ TeV, as obtained from the one-loop improved RG evolution (solid lines) and the analytical formulae (dashed lines). All sets of curves correspond to $\tan \beta = 15$ and large squark mixing, $X_t^2 = 6M_S^2$ ($\mu = 0$).

The case $m_A < M_S$ is a bit more complicated since the effective theory below the supersymmetric scale M_S is the 2HDM. However since radiative corrections in the 2HDM are equally dominated by the top-quark, we can compute analytical expressions based upon the LL approximation at the scale $Q^2 \sim m_t^2$. Our approximation²⁷ differs from the LL all-loop numerical resummation by $\lesssim 3$ GeV, which we consider the uncertainty inherent in the theoretical calculation, provided the mixing is moderate and, in particular, bounded by the condition,

$$\left| \frac{m_{\tilde{t}_1}^2 - m_{\tilde{t}_2}^2}{m_{\tilde{t}_1}^2 + m_{\tilde{t}_2}^2} \right| \lesssim 0.5 \quad (41)$$

where $\tilde{t}_{1,2}$ are the two stop mass eigenstates. In Fig. 12 the Higgs mass spectrum is plotted versus m_A .

Threshold effects

There are two possible caveats in the analytical approximation we have just presented: **i)** Our expansion parameter $\log(M_S^2/m_t^2)$ does not behave properly in the supersymmetric limit $M_S \rightarrow 0$, where we should recover the tree-level result. **ii)** We have expanded the threshold function $\Delta V_{\text{th}}[\phi(M_S)]$ to order X_t^4 . In fact keeping the whole threshold function $\Delta V_{\text{th}}[\phi(M_S)]$ we would be able to go to larger values of X_t and to evaluate the accuracy of the approximation (36) and (40). Only then we will be able to check the reliability of the maximum value of the lightest Higgs mass (which corresponds to the maximal mixing) as provided in the previous sections. This procedure has been properly followed^{27,29} for the most general case $m_Q \neq m_U \neq m_D$. We have proved that keeping the exact threshold function $\Delta V_{\text{th}}[\phi(M_S)]$, and properly running its value from the high scale to m_t with the corresponding anomalous dimensions as in (39), produces two effects: **i)** It makes a resummation from M_S^2 to $M_S^2 + m_t^2$ and generates as (physical) expansion parameter $\log[(M_S^2 + m_t^2)/m_t^2]$. **ii)** It generates a whole threshold function X_t^{eff} such that (40) becomes

$$\Delta_{\text{th}} m_H^2 = \frac{3}{4\pi^2} \frac{m_t^4 [M_S^2 + m_t^2]}{v^2(m_t)} X_t^{\text{eff}} \quad (42)$$

and

$$X_t^{\text{eff}} = \frac{X_t^2}{M_S^2 + m_t^2} \left(2 - \frac{1}{6} \frac{X_t^2}{M_S^2 + m_t^2} \right) + \dots \quad (43)$$

The numerical calculation shows²⁹ that X_t^{eff} has the maximum very close to $X_t^2 = 6(M_S^2 + m_t^2)$, what justifies the reliability of previous upper bounds on the lightest Higgs mass.

2.3 The case of obese supersymmetry

We will conclude this lecture with a very interesting case, where the Higgs sector of the MSSM plays a key role in the detection of supersymmetry. It is the case where all supersymmetric particles are superheavy

$$M_S \sim 1 - 10 \text{ TeV} \quad (44)$$

and escape detection at LHC.

In the Higgs sector \mathcal{H}, A, H^\pm decouple, while the H couplings go to the SM ϕ couplings

$$HXY \longrightarrow (\phi XY)_{\text{SM}} \quad (45)$$

as $\sin(\beta - \alpha) \rightarrow 1$, or are indistinguishable from the SM ones

$$\begin{aligned} h_u \sin \beta &\equiv h_u^{\text{SM}} \\ h_{d,\ell} \cos \beta &\equiv h_{d,\ell}^{\text{SM}} \end{aligned} \quad (46)$$

In this way the $\tan \beta$ dependence of the couplings, either disappears or is absorbed in the SM couplings.

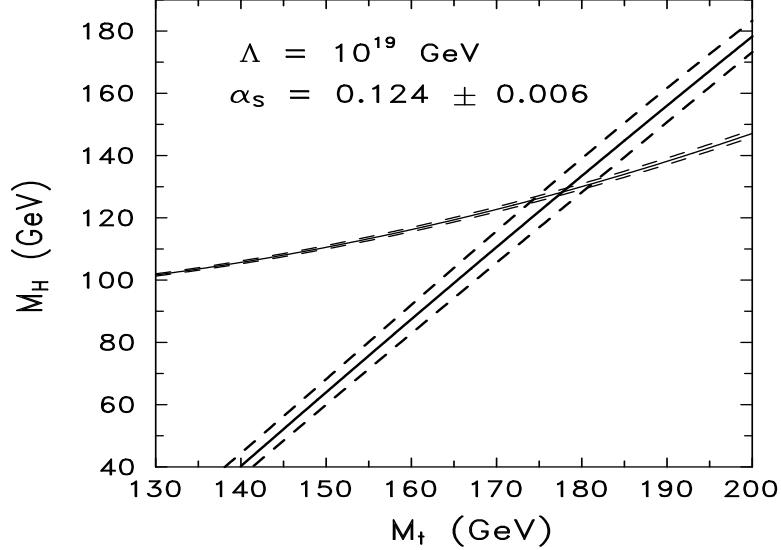


Figure 13: SM lower bounds on M_H (thick lines) as a function of M_t , for $\Lambda = 10^{19}$ GeV, from metastability requirements, and upper bound on the lightest Higgs boson mass in the MSSM (thin lines) for $M_S = 1$ TeV.

However, from the previous sections it should be clear that the Higgs and top mass measurements could serve to discriminate between the SM and its extensions, and to provide information about the scale of new physics Λ . In Fig. 13 we give the SM lower bounds on M_H for $\Lambda \gtrsim 10^{15}$ GeV (thick lines) and the upper bound on the mass of the lightest Higgs boson in the MSSM (thin lines) for $M_S \sim 1$ TeV. Taking, for instance, $M_t = 180$ GeV, close to the central value recently reported by CDF+D0⁹, and $M_H \gtrsim 130$ GeV, the

SM is allowed and the MSSM is excluded. On the other hand, if $M_H \lesssim 130$ GeV, then the MSSM is allowed while the SM is excluded. Likewise there are regions where the SM is excluded, others where the MSSM is excluded and others where both are permitted or both are excluded.

3 Conclusion

To conclude, we can say that the search of the Higgs boson at present and future colliders is, not only an experimental challenge, being the Higgs boson the last missing ingredient of the Standard Model, but also a theoretically appealing question from the more fundamental point of view of physics beyond the Standard Model. In fact, if we are lucky enough and the Higgs boson is detected soon (preferably at LEP2) and *light*, its detection might give sensible information about the possible existence of new physics. In that case, the experimental search of the new physics should be urgent and compelling, since the existence of new phenomena might be necessary for our present understanding of the physics for energies at reach in the planned accelerators.

Acknowledgments

Work supported in part by the European Union (contract CHRX-CT92-0004) and CICYT of Spain (contract AEN95-0195). I wish to thank my collaborators in the subjects whose results are reported in the present lectures: M. Carena, J.A. Casas, J.R. Espinosa, A. Riotto, C. Wagner and F. Zwirner. I also want to thank A. Riotto for his help in drawing some of the diagrams contained in this paper.

References

1. S.L. Glashow, *Nucl. Phys.* **22** (1961)579; S. Weinberg, *Phys. Rev. Lett.* **19** (1967) 1264; A. Salam, *Proc. 8th Nobel Symposium*, Stockholm, 1968, ed. N. Svartholm (Almqvist and Wiksells, Stockholm, 1968), p. 367.
2. P.W. Higgs, *Phys. Rev. Lett.* **12** (1964) 132; and *Phys. Rev.* **13** (1964) 321; F. Englert and R. Brout, *Phys. Rev. Lett.* **13** (1964) 321; G.S. Guralnik, C.R. Hagen and T.W. Kibble, *Phys. Rev. Lett.* **13** (1964) 585.
3. J. Bernabeu, in these proceedings.
4. J.A. Casas, J.R. Espinosa, M. Quirós and A. Riotto, *Nucl. Phys.* **B436** (1995) 3; (E) **B439** (1995) 466.
5. See for instance: K. Aoki, Z. Hioki, R. Kawabe, M. Konuma and T. Muta, *Prog. Theor. Phys. (Suppl.)* **73** (1982) 1.

6. Higgs Physics Working Group (convs. M. Carena and P. Zerwas), in Vol. 1 of *Physics at LEP2*, G. Altarelli, T. Sjostrand and F. Zwirner, eds., Report CERN 96-01, Geneva (1996).
7. A. Ferrando, in these proceedings.
8. Higgs Physics Working Group, in Proceedings of the ECFA Large Hadron Collider Workshop, Vol.II, Aachen (Germany), 4-9 October 1990 (ed. G. Jarlskog and D. Rein), preprint CERN 90-10, ECFA 90-133.
9. F. Abe et al., CDF Collaboration, *Phys. Rev.* **D50** (1994) 2966; *Phys. Rev. Lett.* **73** (1994) 225; *Phys. Rev. Lett.* **74** (1995) 2626; S. Abachi et al., D0 Collaboration, *Phys. Rev. Lett.* **72** (1994) 2138; *Phys. Rev. Lett.* **74** (1995) 2422; *Phys. Rev. Lett.* **74** (1995) 2632.
10. For a recent analysis, see: J. Ellis, G.L. Fogli and E. Lisi, preprint CERN-TH/96-216, and LBNL-39237 [hep-ph/9608329], and references therein.
11. N. Cabibbo, L. Maiani, G. Parisi and R. Petronzio, *Nucl. Phys.* **B158** (1979) 295; M. Lindner, *Z. Phys.* **C31** (1986) 295; M. Sher, *Phys. Rep.* **179** (1989) 273; M. Lindner, M. Sher and H.W. Zaglauer, *Phys. Lett.* **B228** (1989) 139; M. Sher, *Phys. Lett.* **B317** (1993) 159; Addendum: *Phys. Lett.* **B331** (1994) 448; C. Ford, D.R.T. Jones, P.W. Stephenson and M.B. Einhorn, *Nucl. Phys.* **B395** (1993) 17.
12. G. Altarelli and I. Isidori, *Phys. Lett.* **B337** (1994) 141.
13. J.A. Casas, J.R. Espinosa and M. Quirós, *Phys. Lett.* **B342** (1995) 171; J.A. Casas, J.R. Espinosa and M. Quirós, to appear in *Phys. Lett.* **B** (1996), [hep-ph/9603227].
14. J.R. Espinosa and M. Quirós, *Phys. Lett.* **B355** (1995) 257
15. For a recent review, see, e.g.: M. Quirós, *Helv. Phys. Acta* **67** (1994) 451.
16. L. Dolan and R. Jackiw, *Phys. Rev.* **D9** (1974) 3320; S. Weinberg, *Phys. Rev.* **D9** (1974) 3357; D.J. Gross, R.D. Pisarski and L.G. Yaffe, *Rev. Mod. Phys.* **53** (1981) 43; M.E. Carrington, *Phys. Rev.* **D45** (1992) 2933; M.E. Shaposhnikov, *Phys. Lett.* **B277** (1992) 324 and (E) *Phys. Lett.* **B282** (1992) 483; M. Dine, R.G. Leigh, P. Huet, A. Linde and D. Linde, *Phys. Lett.* **B283** (1992) 319 and *Phys. Rev.* **D46** (1992) 550; J.R. Espinosa and M. Quirós, *Phys. Lett.* **B305** (1993) 98; J.R. Espinosa, M. Quirós and F. Zwirner, *Phys. Lett.* **B314** (1993) 206; C.G. Boyd, D.E. Brahm and S.D. Hsu, *Phys. Rev.* **D48** (1993) 4963; P. Arnold and O. Espinosa, *Phys. Rev.* **D47** (1993) 3546; W. Buchmüller, T. Helbig and D. Walliser, *Nucl. Phys.* **B407** (1993) 387.
17. A.D. Linde, *Phys. Lett.* **B70** (1977) 306; *Phys. Lett.* **B100** (1981) 37; *Nucl. Phys.* **B216** (1983) 421.
18. S. Coleman, *Phys. Rev.* **D15** (1977) 2929.
19. P. Arnold and S. Vokos, *Phys. Rev.* **D44** (1991) 3620.

20. H.P. Nilles, *Phys. Rep.* **110** (1984) 1; H.E. Haber and G.L. Kane, *Phys. Rep.* **117** (1985) 75; R. Barbieri, *Riv. Nuovo Cim.* **11** (1988) 1.
21. C. Wagner, in these proceedings.
22. See, e.g. J.F. Gunion, H.E. Haber, G.L. Kane and S. Dawson, *The Higgs Hunter's Guide*, Addison-Wesley 1990.
23. Z. Kunszt and F. Zwirner, *Nucl. Phys.* **B385** (1992) 3.
24. Y. Okada, M. Yamaguchi and T. Yanagida, *Prog. Theor. Phys.* **85** (1991) 1; *Phys. Lett.* **B262** (1991) 54; J. Ellis, G. Ridolfi and F. Zwirner, *Phys. Lett.* **B257** (1991) 83; *Phys. Lett.* **B262** (1991) 477; R. Barbieri and M. Frigeni, *Phys. Lett.* **B258** (1991) 395; R. Barbieri, M. Frigeni and F. Caravaglios, *Phys. Lett.* **B258** (1991) 167.
25. J.R. Espinosa and M. Quirós, *Phys. Lett.* **B266** (1991) 389.
26. H.E. Haber and R. Hempfling, *Phys. Rev. Lett.* **66** (1991) 1815; A. Yamada, *Phys. Lett.* **B263** (1991) 233.
27. M. Carena, J.R. Espinosa, M. Quirós and C.E.M. Wagner, *Phys. Lett.* **B355** (1995) 209.
28. H.E. Haber, R. Hempfling and A.H. Hoang, preprint CERN-TH/95-216, and TTP95-09 (1995) [hep-ph/9609331].
29. M. Carena, M. Quirós and C.E.M. Wagner, *Nucl. Phys.* **B461** (1996) 407.